ISSN: 2581-1274

Assessment of Geodetic Mission Satellite Altimeter Sea Surface Height Data for Developing Marine Gravity Anomaly Models

Akbar Wahyu Nugraha [a,1,*], Dudy Darmawan Wijaya [b,2]

[a] *Department of Geomatics Engineering, Institute of Technology Sumatera, Jl. Terusan Ryacudu, Lampung Selatan 35365, Indonesia*
[b] *Department of Geodesy and Geomatics Engineering, Institut Teknologi Bandung, Jl. Ganesha 10, Bandung, 40116, Indonesia*
[1]*akbar.nugraha@gt.itera.ac.id*;* [2] *dudy.wijaya@itb.ac.id*
*corresponding author

ARTICLE INFO

Article history:
Published

Keywords:
Satellite Altimetry
Sea Surface Height
Deflection of Vertical
Marine Gravity Anomaly
Inverse Vening Meinesz

ABSTRACT

Marine gravity anomalies are critical for various applications, including the analysis of oceanic faults, bathymetry prediction, and the development of marine geoids. These anomalies can be measured using shipborne and airborne gravimetry, both of which offer high accuracy and resolution but are limited by their spatial coverage. Conversely, satellite altimetry provides comprehensive global coverage, making it a valuable tool for studying marine gravity anomalies on a larger scale. This research investigates the effectiveness of satellite altimetry in generating marine gravity anomaly data for the eastern Indonesian seas (6°N-6°S and 115°E-135°E). The study employs spectral analysis of Sea Surface Height (SSH) data to identify dominant components and their spatial resolution. Subsequently, the SSH data is used to calculate marine gravity anomalies via the Inverse Vening Meinesz (IVM) method. The accuracy of these satellite-derived anomalies is validated against shipborne gravimetry measurements. Results indicate that satellite altimetry can produce marine gravity anomalies with an accuracy ranging from 4.130 to 9.547 mGal and a spatial resolution of 11.75 kilometres.

I. Introduction

Marine gravity anomaly is a critical parameter with applications in various fields, notably geophysics and geodesy. In geophysics, marine gravity anomalies are invaluable for geological structure analysis [1], sediment basin delineation [2], and fault analysis in marine areas [3]. In geodesy, marine gravity anomalies play a pivotal role in bathymetry prediction [4][5][6] and marine geoid determination [7][8]. Several methods exist for determining gravity anomalies in the ocean, including shipborne gravimetry, airborne gravimetry, and satellite altimetry [9]. Shipborne and airborne gravimetry offer high accuracy and resolution, providing detailed local data. However, they are limited by their regional coverage, requiring extensive time and resources to cover large areas [10][11]. In contrast, satellite altimetry provides global coverage, allowing for the collection of extensive data over vast oceanic regions. This method has revolutionized the study of the marine gravity field by offering freely accessible data that can be used to enhance our understanding of ocean dynamics and Earth's gravity field [12]. To fully leverage the potential of satellite altimetry in producing marine gravity anomaly values, it is crucial to conduct comprehensive analyses of the resolution and accuracy of satellite altimetry data.

The satellite altimetry data utilized to generate marine gravity anomalies is derived from Sea Surface Height (SSH) measurements obtained from satellite altimetry geodetic missions [12]. SSH data encompasses several critical components: long-wavelength geoid undulations, short-wavelength geoid undulations, Mean Dynamic Topography (MDT), and Dynamic Ocean Topography (DOT) [9]. Among these components, the short-wavelength geoid undulations are specifically used in the calculation of marine gravity anomalies. Short-wavelength geoid undulations are then used to determine vertical deflection [9].

The vertical deflection obtained is then converted into marine gravity anomalies using the Inverse Vening Meinesz (IVM) method [13]. The resulting marine gravity anomalies are validated against marine gravity anomaly data measured using shipborne gravimetry, that obtained from the National Geophysical Data Center (NGDC). This validation process helps determine the accuracy and reliability of the generated marine gravity anomaly model compared to shipborne measurement data. Furthermore, to assess the optimal spatial resolution of the generated marine gravity anomaly model, the marine gravity anomalies are transformed from the spatial domain to the spectral domain using the Fast Fourier Transform (FFT) method [14]. In the spectral domain, the shortest wavelength, which indicates the optimal resolution, and the signal strength can be identified.

This study leverages data from four geodetic satellite altimetry missions: Cryosat-2 phase A, Jason-1 phase C, SARAL phase B, and ERS-1 phase F. The Sea Surface Height (SSH) data utilized spans the eastern Indonesian maritime region, specifically between 6°N-6°S latitude and 115°E-135°E longitude. This region was selected for its intricate and diverse characteristics, making it an ideal area for detailed analysis [27]. The eastern Indonesian maritime area is characterized by numerous narrow waterways, small islands, and highly variable seabed conditions. These features present a unique opportunity to rigorously test the reliability of satellite altimetry and perform a comprehensive analysis of the marine gravity anomaly model. The complexity of the region ensures that the evaluation is thorough, encompassing a wide range of environmental conditions and challenges.

In conclusion, this study will perform a comprehensive spectral analysis on Sea Surface Height (SSH) data to pinpoint the dominant components and their corresponding spatial resolutions. This detailed examination will provide insights into the most significant elements within the SSH data. Following this, the SSH data will be employed to calculate marine gravity anomalies through the Inverse Vening Meinesz (IVM) method. The generated marine gravity anomalies will undergo rigorous validation against shipborne gravimetry data obtained from the National Geophysical Data Center (NGDC). This validation process will be crucial for assessing the accuracy and reliability of the marine gravity anomaly model.

II. Method

In this study, the marine gravity anomaly model is constructed using Sea Surface Height (SSH) data obtained from four satellite altimetry missions: Cryosat-2 phase A, Jason-1 phase C, SARAL phase B, and ERS-1 phase F. The SSH data spans the eastern Indonesian maritime region (6°N-6°S and 115°E-135°E) and is sourced from the Radar Altimeter Database System (RADS). The SSH data contains information on geoid undulations (N) and Sea Surface Topography (SST), as illustrated in Figure 1 [15].

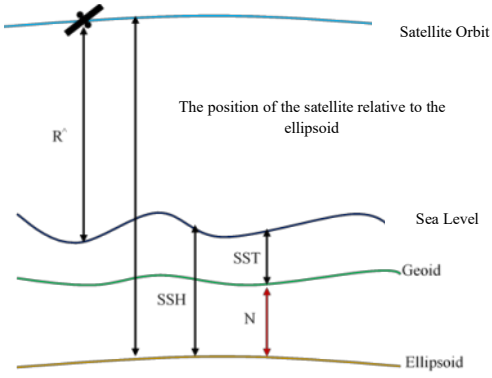

Fig. 1. The Relationship Between SSH, Geoid Undulation (N), and SST

Mathematically, Sea Surface Height (SSH) is defined as the sum of geoid undulation (N) and Sea Surface Topography (SST), as represented in equation (1) below:

$$SSH = N + \zeta + e \quad (1)$$

where N is the geoid undulation, ζ is the SST, and e is the error.

Additionally, both geoid undulation and Sea Surface Topography (SST) are comprised of distinct components. Geoid undulation is divided into a long-wavelength component (Nref), which serves as a reference, and a short-wavelength component (Nres), representing residual variations [9]. SST is further subdivided into mean dynamic topography (ζMDT) and time-varying sea surface topography (ζ(t)), that also referred to as dynamic ocean topography (DOT) [16]. Consequently, equation (1) can be detailed and redefined in equation (2) [9].

$$SSH = N_{ref} + N_{res} + \zeta_{MDT} + \zeta(t) + e \tag{2}$$

The information required for determining marine gravity anomalies is the residual geoid undulation (Nres) [17]. Therefore, the components Nref, ζMDT, and DOT need to be removed first. These components represent long-wavelength signals, and thus their values will be nearly identical at adjacent points [9]. Consequently, when the SSH values at two adjacent points are differenced, the long-wavelength components Nref, ζMDT, and DOT will cancel out from equation (2), as their difference can be considered negligible. Thus, the remaining component in equation (2) is the residual geoid undulation (Nres). In addition to removal, the effect of DOT on SSH data is also mitigated through geophysical correction processes during data download and filtering [18]. SSH data filtering is performed using a 1-D Gaussian filter [19]. Subsequently, the gradient of the residual undulation (ΔNres), which represents the difference in residual geoid undulation values, can be approximated from the SSH data using equation (3) provided below:

$$\frac{SSH_2 - SSH_1}{d} \approx \frac{Nres_2 - Nres_1}{d} \tag{3}$$

The vertical deflection is calculated at each crossover point, defined as the intersection where ascending and descending satellite tracks converge (Figure 2).

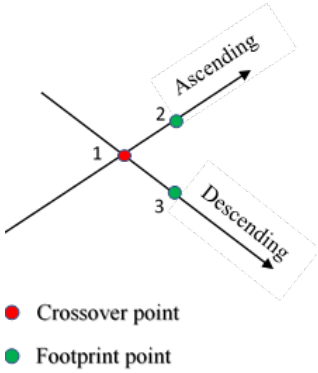

Fig. 2. *Ascending*, *Descending*, and *Crossover Point*

Vertical deflection at each crossover point is calculated using the gradient of undulation data obtained from both the ascending (equation 4) and descending (equation 5) satellite tracks.

$$\frac{SSH_2 - SSH_1}{d} \approx \frac{N_{res2} - N_{res1}}{d} \tag{4}$$

$$\frac{SSH_3 - SSH_1}{d} \approx \frac{N_{res3} - N_{res1}}{d} \tag{5}$$

Vertical deflection in the north-south direction (ξ), which reflects the vertical deflection along the latitude (φ), and vertical deflection in the east-west direction (η), corresponding to the vertical deflection along the longitude (λ), are derived from undulation gradient data in both latitude and longitude directions. To achieve this, interpolation of the undulation gradient values is required to generate a comprehensive grid. This grid incorporates detailed information on the gradients in both the latitude and longitude directions.

Once the data is formatted into a grid, the undulation gradient at crossover points in the latitude direction $\left(\frac{\partial N_1}{\partial_\varphi}\right)$ is employed to calculate the vertical deflection in the north-south direction (ξ) as described in equation (6). Similarly, the undulation gradient at crossover points in the longitude

direction $\left(\frac{\partial N_1}{\partial_\lambda}\right)$ is used to determine the vertical deflection in the east-west direction (η) as described in equation (7).

$$\xi_1 = -\frac{1}{R}\frac{\partial N_1}{\partial_\varphi} \tag{6}$$

$$\eta_1 = -\frac{1}{Rcos\varphi}\frac{\partial N_1}{\partial_\lambda} \tag{7}$$

Marine gravity anomalies are derived from vertical deflections in both the north-south direction (ξ) and east-west direction (η) using the Inverse Vening Meinesz (IVM) method [13]. This equation is employed to convert vertical deflection into gravity anomaly $\Delta\mathbf{g}$. Advances in satellite altimetry have made vertical deflection data over the ocean widely available, thereby enhancing the efficacy of the IVM method for calculating marine gravity anomalies in marine environments. To determine the gravity anomaly (Δg) at a specific location within the study area, the IVM method integrates vertical deflection data from the entire region. Consequently, vertical deflections are provided in a grid format with a resolution of 1' x 1'. The calculation of marine gravity anomalies using the IVM method is performed according to equation (8) [13].

$$\Delta\mathbf{g}_p = \frac{1}{4\pi\gamma}\iint K_{(\psi_{pq})}\left(\xi_q cos\alpha_{qp} + \eta_q sin\alpha_{qp}\right)d\sigma_q \tag{8}$$

with $\Delta\mathbf{g}_p$ = gravity anomaly at point p, γ = normal gravity, ψ_{pq} = spherical distances p and q, (ξ_q, η_q) = deflections in the north-south direction at q, α_{qp} = azimuth from q to p, $d\sigma_q$ = surface element $(cos\,\varphi_q d\varphi_q d\lambda_q)$, dan $K_{(\psi_{pq})}$ = kernel function between points p and q, with:

$$K_{(\psi_{pq})} = \frac{\cos(\psi_{pq}/2)}{2\sin(\psi_{pq}/2)}\left(-\frac{1}{\sin(\psi/2)} + \frac{3+2\sin(\psi_{pq}/2)}{1+\sin(\psi_{pq}/2)}\right) \tag{9}$$

In this study, the IVM equation for determining marine gravity anomalies will be addressed through spectral analysis utilizing the one-dimensional Fast Fourier Transform (FFT 1-D) method. This approach involves decomposing equation (8) into [20]:

$$\Delta\mathbf{g}\varphi_p(\lambda_p) = \frac{1}{4\pi\gamma}\sum_{\varphi_q=\varphi_1}^{\varphi_n}\left(K_{(\psi_{pq})}(\Delta\lambda_{qp})\right)x\left(\xi_q cos\alpha_{qp} + \eta_q sin\alpha_{qp}\right)(cos\,\varphi\Delta\varphi\Delta\lambda) \tag{10}$$

$$\Delta\mathbf{g}\varphi_p(\lambda_p) = \frac{\Delta\varphi\Delta\lambda}{4\pi\gamma}\,\boldsymbol{F_1^{-1}}\left(\sum_{\varphi_q=\varphi_1}^{\varphi_n}\boldsymbol{F_1}\left(K_{(\psi_{pq})}(\Delta\lambda_{qp})cos\alpha_{qp}\right)\boldsymbol{F_1}(\xi\cos\varphi) + \boldsymbol{F_1}\left(K_{(\psi_{pq})}(\Delta\lambda_{qp})sin\alpha_{qp}\right)\boldsymbol{F_1}(\eta\cos\varphi)\right) \tag{11}$$

In equation (11), each component, such as the kernel function $K_{(\psi_{pq})}$ and the vertical deflections in the north (ξ) and east (η) directions, is first transformed into the spectral domain using one-dimensional FFT-1D ($\boldsymbol{F_1}$) along the latitude lines. Subsequently, the vertical deflections in the north (ξ) and east (η) directions are convolved with the kernel function. After convolution with the kernel function, the vertical deflections in the north and east directions are summed. Finally, the result of this summation is transformed back into the spatial domain using the inverse FFT-1D ($\boldsymbol{F_1^{-1}}$), yielding the gravity anomaly in the spatial domain.

Due to the singularity of the kernel function $K(\psi)$ at a spherical distance of zero (ψ_{pp}), marine gravity anomalies arising from vertical deflection contributions at the same point (innermost zone effects) are calculated separately using equation (12), and then combined with the marine gravity anomalies from the outermost zone contributions,

$$\Delta\mathbf{g}_i = \frac{1}{2}s_o\gamma(\xi_y + \eta_x) \tag{12}$$

dengan,

$$s_o = \sqrt{\frac{\Delta x+\Delta y}{\pi}} \tag{13}$$

III. Results and Discussion

A. Assessment of Sea Surface Height Data Resolution

Resolution testing of SSH data aims to ascertain the maximum spatial resolution of the marine gravity anomaly model derived from SSH data. This testing involves analyzing the dominance of the physical components constituting the SSH data. This step is crucial as the physical components within the SSH data significantly influence the quality of the resultant marine gravity anomaly model. The specific physical components present in the SSH data utilized in this study are depicted in Figure 3 below.

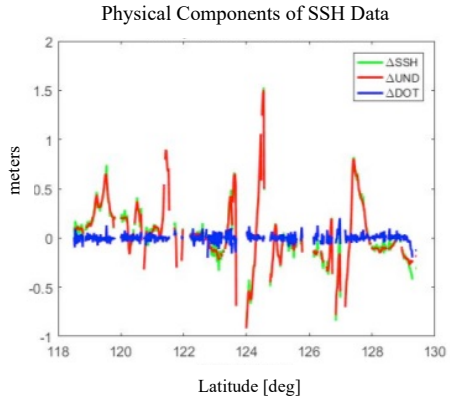

Fig. 3. Physical Components of SSH Data (ΔSSH = red, ΔUndulation = blue, ΔDOT = green).

In Figure 3, it can be observed that the SSH data still contains dynamic ocean topography (DOT). This indicates that the filtering process performed was not entirely effective in eliminating DOT. Although DOT appears to be minor in Figure 3, its effects must be minimized as much as possible to obtain the true gravity anomaly values. In gravity anomaly modeling, DOT is considered noise that must be reduced.

To determine the dominance and signal strength of each physical component of SSH as well as the resulting resolution, a transformation to the spectral domain is necessary. This transformation is carried out using the fast Fourier transformation (FFT) method [14]. In the spectral domain, the physical components of SSH can be seen in Figure 4 below.

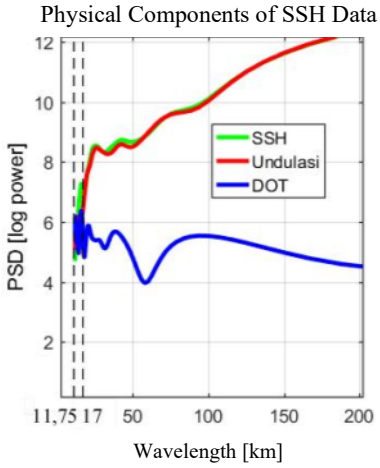

Fig. 4. Physical Components of SSH Data in the Spectral Domain

Based on Figure 4, the undulation signal graph aligns more closely with the SSH signal graph compared to the DOT signal graph. This indicates that the undulation signal is more dominant as a physical component of the SSH data than the DOT signal. In the wavelength range of 11.75 – 17 kilometers, the DOT signal graph appears to align with the SSH signal graph, suggesting that within this wavelength range, the SSH data is still contaminated by DOT. However, at wavelengths greater than 17 kilometers, the DOT signal graph no longer aligns with the SSH signal graph, indicating that

the influence of DOT on the SSH data is minimal. The wavelength, represented on the x-axis of the graph in Figure 5, indicates the spatial resolution of the SSH data. Therefore, based on the graph, it can be inferred that altimetry satellites are capable of providing SSH data with a resolution of approximately 11.75 kilometers (>6 minutes). In other words, the SSH data provided by altimetry satellites can be used to develop a gravity anomaly model with a resolution of up to approximately 11.75 kilometers.

Since the SSH data still contains DOT components, filtering using the Gaussian 1-D filter method is necessary to reduce the influence of the DOT components [20]. After filtering, the data is used to calculate the undulation gradient. The spectral profile of the undulation gradient can be seen in Figure 5 below.

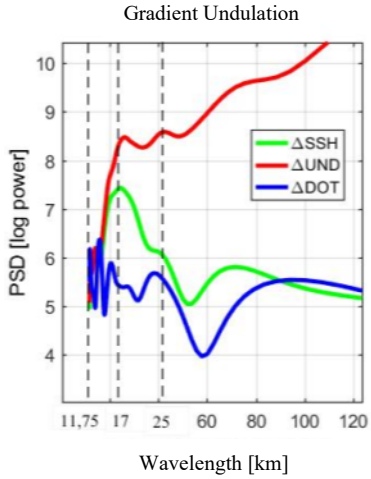

Fig. 5. Physical Components of Gradient Undulation in the Spectral Domain

The spectral profile of a component represents the distribution of its signal strength across different wavelengths, which, in turn, indicates the magnitude of the component's values. In Fig. 5, it can be observed that in the wavelength range of 11.75 – 17 kilometers, the spectral profile of undulation aligns with the spectral profile of SSH, whereas the spectral profile of DOT appears to be the opposite. This indicates that the undulation values are more similar to the SSH values compared to the DOT values. It is important to remember that SSH is the sum of undulation and DOT. Therefore, as one component becomes more prominent, the influence of the other component diminishes. In other words, in the wavelength range of 11.75 – 17 kilometers, the influence of the undulation component on SSH is stronger than that of the DOT component. In the wavelength range of 17 – 25 kilometers, the influence of DOT on SSH data decreases, as indicated by the DOT spectral profile diverging from the SSH spectral profile. However, beyond this range, the influence of DOT on SSH data strengthens and becomes more dominant than the undulation component at wavelengths above 25 kilometers. At wavelengths greater than 100 kilometers, the DOT frequency density closely resembles SSH, indicating that at these wavelengths, DOT values are nearly identical to SSH. Thus, it can be concluded that the influence of DOT on SSH data varies across different wavelengths. The presence of DOT influence demonstrates that the filtering process applied to the SSH data has not optimally removed DOT.

The undulation gradient, still containing DOT, is then used to calculate the vertical deflection components in the north and south directions, as previously described. One advantage of using vertical deflection for determining marine gravity anomalies, compared to the undulation gradient, is that vertical deflection is less contaminated by long-wavelength errors, particularly DOT [9]. Vertical deflection is determined at each crossover point, which is the intersection point between ascending and descending tracks. The obtained vertical deflection is then used to determine marine gravity anomalies using the IVM method.

B. Accuracy of Marine Gravity Anomaly Models

Based on calculations performed using the IVM method, a gravity anomaly model in the form of a grid with a spatial resolution of one minute (~2 km) was obtained, as shown in the Figure 6.

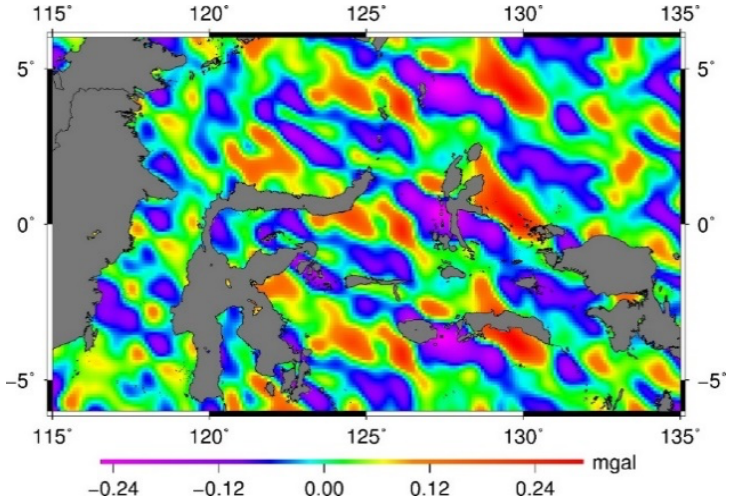

Fig. 6. Short-Wavelength Marine Gravity Anomaly Model.

In the figure, there are no wave formations or spots resembling orange peel on the marine gravity anomaly, which would indicate the presence of DOT components. The failure to reduce DOT would cause an "orange skin effect" on the resulting marine gravity anomaly model [21][22]. This indicates that the influence of DOT components has been successfully minimized by calculating the vertical deflection. The calculated marine gravity anomaly, as shown in Fig. 6, contains only short-wavelength information. To obtain a complete marine gravity anomaly profile, it must be supplemented with long-wavelength information from the EGM2008 marine gravity anomaly model. The marine gravity anomaly after incorporating the long-wavelength information from EGM2008 is shown in Figure 7 below.

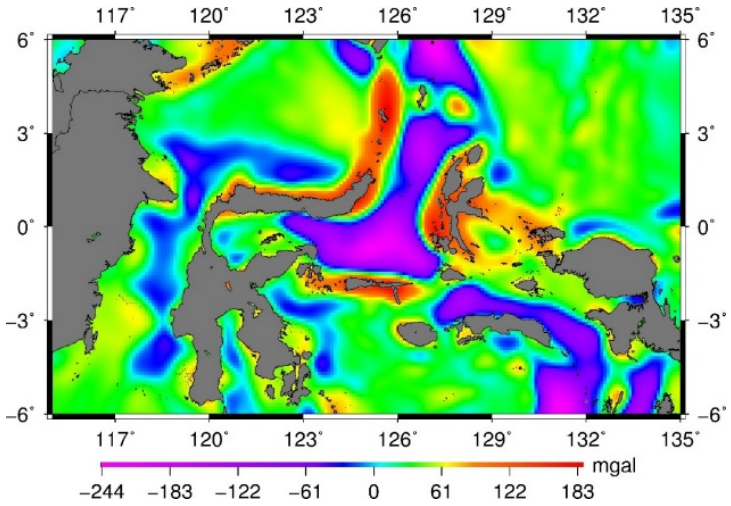

Fig. 7. Full-Wavelength Marine Gravity Anomaly Model

Accuracy testing is performed by comparing the calculated marine gravity anomaly (IVM gravity anomaly) with the measured marine gravity anomaly using shipborne data (shipborne gravity anomaly). The accuracy of the IVM marine gravity anomaly is indicated by the Root Mean Square Error (RMSE) value, which represents the comparison between the IVM marine gravity anomaly and the shipborne data.

The shipborne data distribution is random, so it does not cover the entire study area. On the other hand, the IVM marine gravity anomaly is already in the form of a grid with a spatial resolution of one minute. Since the spatial resolutions of the two data sets differ, one of the data sets needs to be interpolated to match the other. To maintain the integrity of the shipborne data as validation data, the accuracy test is performed according to the shipborne measurement tracks. Therefore, the IVM marine gravity anomaly values along the shipborne measurement tracks are approximated by interpolation, and these measurement tracks can be seen in Figure 8. The interpolation is performed using the cubic interpolation method [23].

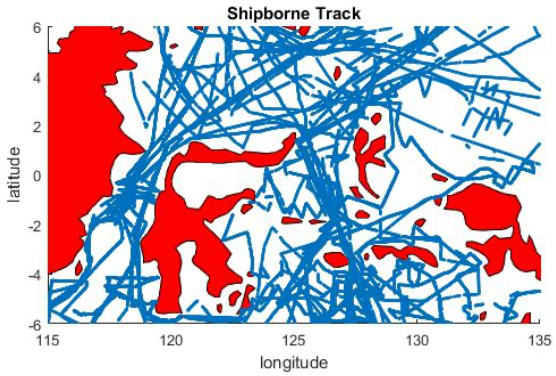

Fig. 8. Shipborne Measurement Track

The accuracy test performed across the entire shipborne measurement track involves comparing cross-sectional profiles of the full-wavelength IVM marine gravity anomaly (EGM2008+Altimetry) with the shipborne marine gravity anomaly. This comparison, including the associated deviations, is illustrated in Figure 9. Overall, the IVM marine gravity anomaly along the shipborne measurement track exhibits a Root Mean Square Error (RMSE) of 9.547 mGal.

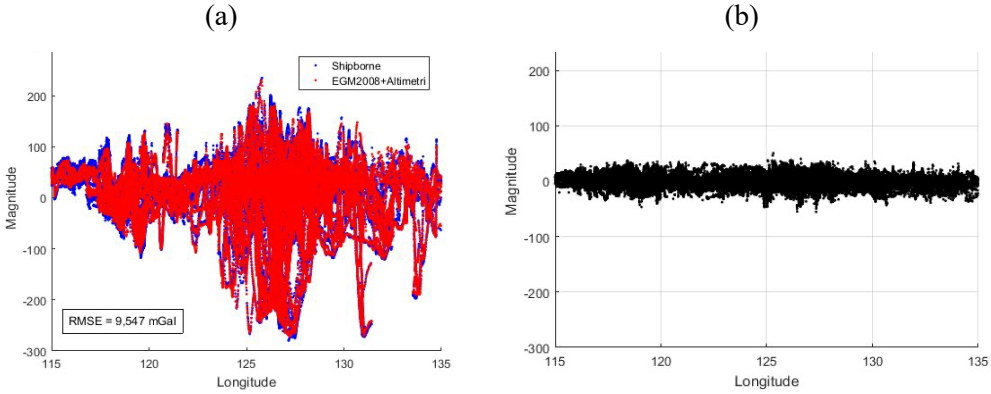

Fig. 9. Cross-Sectional Profile Differences of Full-Wavelength Marine Gravity Anomaly (a) and Its Deviations (b)

To gain a more detailed understanding of the regions with the largest deviations, accuracy testing will also be conducted along specific routes. These include track 1 and track 2, selected based on regional characteristics. Track 1 passes through numerous coastal areas, whereas track 2 traverses fewer coastal regions. The locations of these two tracks are illustrated in Figure 10 below.

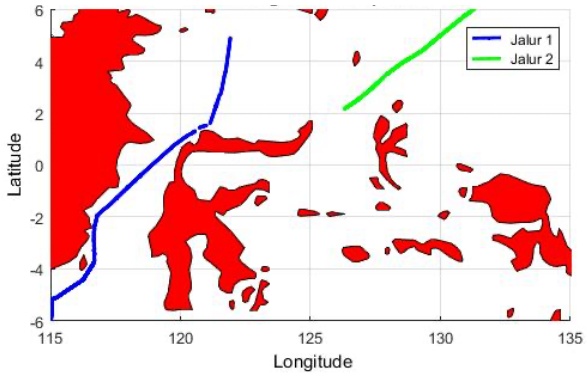

Fig. 10. Locations of Track 1 (blue) and Track 2 (green)

The comparison of cross-sectional profiles of the full-wavelength marine gravity anomaly, along with their deviations, for track 1 and track 2 can be seen in Fig. 11 and 12.

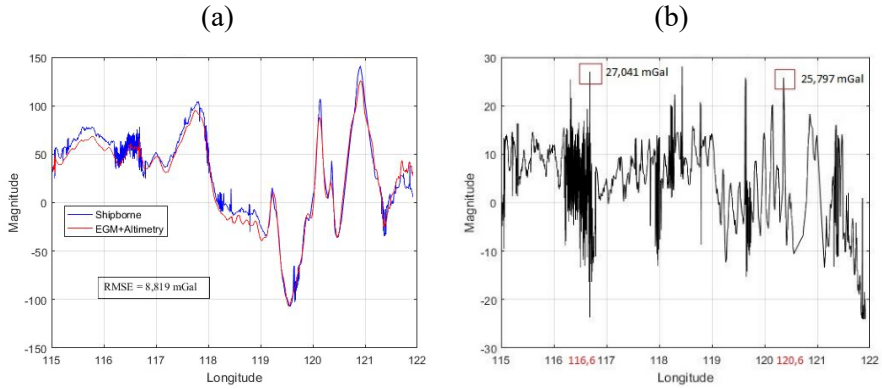

Fig. 11. Cross-Sectional Profiles of EGM2008+Altimetry and Shipborne Marine Gravity Anomaly (a) and Their Deviations (b) Along Track 1.

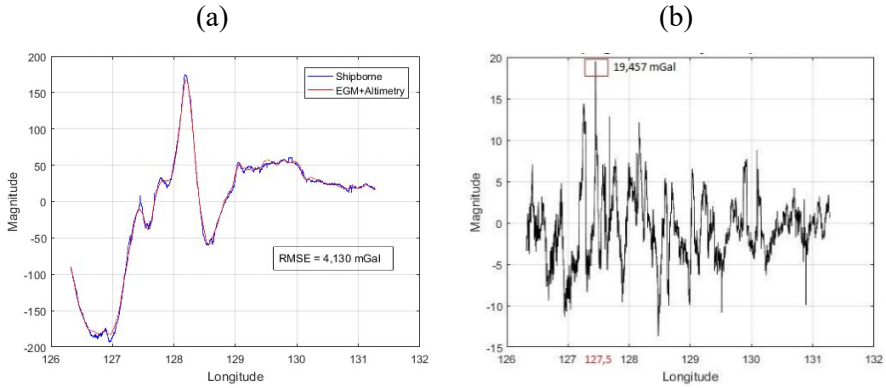

Fig. 12. Cross-Sectional Profiles of EGM2008+Altimetry and Shipborne Marine Gravity Anomaly (a) and Their Deviations (b) Along Track 2.

Based on Figures 11 and 12, it can be observed that the marine gravity anomaly profile calculated with higher alignment to the shipborne data is from track 2. This is further supported by the smaller RMSE for the marine gravity anomaly on track 2 (4.130 mGal) compared to the RMSE on track 1 (8.8 mGal). This indicates that regional characteristics can influence the quality of the resulting marine gravity anomaly.

Notably, several locations on track 1 show marine gravity anomalies with significant deviations (see Fig. 11b), such as at longitudes 116.6° and 120.6°, with deviations of 27.041 mGal and 25.8 mGal, respectively. Similarly, track 2 has a notable anomaly at longitude 127.5°, with a deviation of 19.5 mGal. These three locations share a common characteristic, they are all situated near coastal areas (see Fig. 13).

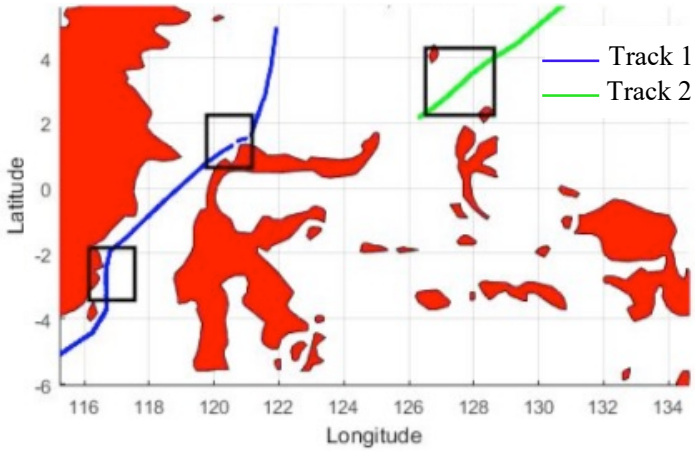

Fig. 13. Locations of Shallow Waters Traversed by Track 1 and Track 2

Coastal areas or shallow waters are known to be a weakness for altimetry satellites [24]. These regions, the emitted waves encounter land or are at least influenced by it. The presence of land means that the waves emitted by the altimeter are not fully reflected back, as some of the waves are absorbed by the land [24]. Consequently, the characteristics of the reflected waves do not match the expected Brown waveform characteristics [24]. The altimetry system only accepts waves that conform to the Brown waveform, so waves contaminated by land are not captured by the altimetry system. As a result, there will be gaps in the SSH data in regions affected by land. This indicates that areas with large marine gravity anomaly deviations are those where the marine gravity anomalies are derived from interpolated SSH data.

This issue is not trivial and should not be ignored. Data gaps in coastal regions can result in poor-quality marine gravity anomalies in these areas. However, marine gravity anomaly data in coastal areas is crucial for determining the geoid as a singular vertical reference system. This study will not delve further into the impact of land on SSH data quality. For future research, it is recommended to reduce the impact of land on SSH data by performing re-tracking and/or combining it with shipborne gravimetry data.

Re-tracking is the process of re-tracking waveforms that do not conform to the Brown waveform. Re-tracking is done by expanding the tolerance of the Brown waveform, thereby increasing the number of acceptable waveforms, which implies an increase in the amount of SSH data [25]. Re-tracking is performed twice, also known as double re-tracking. The first re-tracking aims to increase the amount of SSH data, while the second aims to improve the accuracy of the SSH data [26]. After re-tracking, gravity accuracy in coastal and polar regions improves by 40-50% compared to previous gravity models [25]. In this study, the SSH data used did not undergo re-tracking, but it is recommended that future research use SSH data that has undergone re-tracking. Additionally, improving the quality of marine gravity anomalies can also be achieved by combining SSH data with shipborne marine gravity anomaly data.

Combining with shipborne data not only enhances the accuracy of marine gravity anomaly data in coastal regions but also improves its spatial resolution. This improvement in spatial resolution is possible because shipborne data has a higher spatial resolution compared to the marine gravity anomaly model. This is illustrated by the closer fluctuations in shipborne data compared to the marine gravity anomaly graph, as shown in Figure 14.

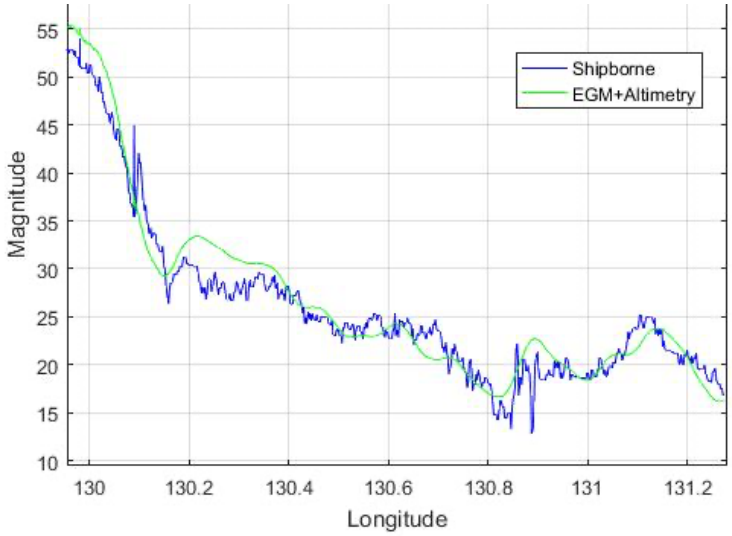

Fig. 14. Comparison of the Fluctuations Between Shipborne Data Graphs and IVM Marine Gravity Anomaly (EGM2008 + Altimetry) Graphs.

C. Resolution of Marine Gravity Anomaly Models

Resolution testing is carried out through a spectral analysis of the full-wavelength IVM marine gravity anomaly (Altimetry + EGM2008) and the shipborne marine gravity anomaly in the spectral domain, as illustrated in Figure 15 below.

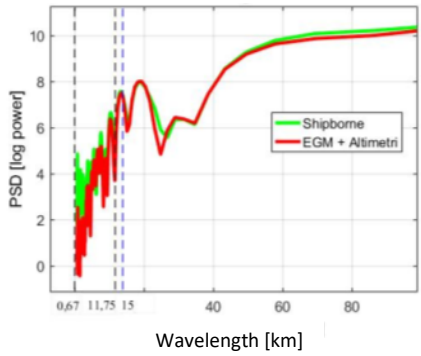

Fig. 15. Spectral Profile of Full-Wavelength Marine Gravity Anomaly

Based on Figure 15, it can be observed that shipborne data can provide marine gravity anomaly data with a spatial resolution of up to 0.677 kilometers (21.9 seconds). Additionally, altimetric SSH data also appears capable of producing a marine gravity anomaly model with a resolution of up to 0.677 kilometers, matching the spatial resolution of shipborne marine gravity anomalies. However, in reality, this is not the case, the marine gravity anomaly model produced involves interpolation in its creation. Furthermore, during validation, interpolation is carried out along the shipborne measurement tracks, resulting in a spatial resolution equivalent to that of the shipborne marine gravity anomalies. The actual spatial resolution of the marine gravity anomaly model is the resolution during the SSH data resolution test, which is approximately 11.75 kilometers or about 6 minutes.

The figure shows that the Power Spectrum Density (PSD) of the spectral profiles of the altimetric marine gravity anomaly and shipborne gravity anomaly differs at each wavelength. At wavelengths below 11.75 kilometers, the spectral profile of the shipborne marine gravity anomaly exhibits a higher PSD compared to the altimetric gravity anomaly. This indicates that shipborne measurements are better at capturing marine gravity anomaly information with wavelengths shorter than 11.75 kilometers than altimetry. Additionally, the lower PSD of altimetry at wavelengths below 11.75 kilometers may be due to the signal being obscured by noise caused by land effects. At wavelengths above 15 kilometers, the PSD values of the spectral profiles of both shipborne and altimetric marine gravity anomalies tend to converge. This suggests that altimetry has similar capabilities to shipborne measurements in capturing marine gravity anomaly signals with wavelengths longer than 15 kilometers. Moreover, this study also provides information that the ability of a platform to capture marine gravity anomaly information is related to its spatial resolution. The wavelength information that can be captured is twice the spatial resolution of the platform. For example, the Cryosat-2 altimeter satellite has a spatial resolution of up to 7 kilometers, so it effectively captures marine gravity anomaly information with wavelengths longer than 14 kilometers. This is why the PSD of the altimetric gravity anomaly spectral profile increasingly aligns with the shipborne spectral profile at wavelengths above 15 kilometers. Additionally, the differences in signal strength between the two platforms highlight the need for data combination, allowing for the creation of a marine gravity anomaly model with resolutions between 11.75 and 0.677 kilometers.

IV. Conclusion

The SSH data used has a spatial resolution of approximately 11.75 kilometers. The filtering process using a 1-D Gaussian filter has not fully removed the influence of DOT. As a result, the undulation gradient, that derived from the SSH data, still contains DOT, especially at spatial resolutions above 25 kilometers. The influence of DOT can only be minimized so that it does not appear in the marine gravity anomaly model when calculating vertical deflection. The marine gravity anomaly model derived from SSH data has a spatial resolution of approximately 11.75 kilometers, while the shipborne marine gravity anomaly model has a spatial resolution of 0.67 kilometers. The RMSE of the gravity anomaly model compared to the shipborne marine gravity anomaly data ranges from 4.130 to 9.547 mGal, influenced by coastal bias.

To improve the spatial resolution of the marine gravity anomaly, it is necessary to combine SSH data with shipborne marine gravity anomaly data to develop a gravity anomaly model with a spatial resolution of up to 0.67 kilometers or approximately 21.6 seconds. To enhance the accuracy of the

marine gravity anomaly, re-tracking of the altimetric satellite SSH data in coastal areas is needed to minimize bias due to land effects. In addition to re-tracking, the influence of coastal regions can also be reduced by combining SSH data with shipborne marine gravity anomaly data. This is achieved by limiting the altimetry work area to a specific radius from the land and using shipborne marine gravity anomaly data to fill the gaps in the altimetry data.

References

[1] D. Darisma, M. Marwan, and N. Ismail, "Geological Structure Analysis of Satellit Gravity Data in Oil and Gas Prospect Area of West Aceh-Indonesia," *Journal of Aceh Physics Society*, vol. 8, no. 1, pp. 1–5, 2019.

[2] M. Yanis, "The potential use of satellite gravity data for oil prospecting in Tanimbar Basin, Eastern Indonesia," in *IOP Conference Series: Earth and Environmental Science*, IOP Publishing, 2019, p. 012032.

[3] Y. Muhammad, A. Faisal, A. Yenny, Z. Muzakir, M. Abubakar, and I. Nazli, "Continuity of great sumatran fault in the marine area revealed by 3D inversion of gravity data," *J Teknol*, vol. 83, no. 1, pp. 145–155, 2020.

[4] X. Wan, J. Ran, and S. Jin, "Sensitivity analysis of gravity anomalies and vertical gravity gradient data for bathymetry inversion," *Marine geophysical research*, vol. 40, pp. 87–96, 2019.

[5] C. Yuan, X. Sui, R. Zhang, S. Shi, and H. Zhang, "Bathymetry prediction in Mariana Trench seabed terrain based on altimetry gravity anomalies and vertical gravity gradients," in *International Conference on Remote Sensing, Surveying, and Mapping (RSSM 2024)*, SPIE, 2024, pp. 105–114.

[6] Z. Sun, M. Ouyang, and B. Guan, "Bathymetry predicting using the altimetry gravity anomalies in South China Sea," *Geod Geodyn*, vol. 9, no. 2, pp. 156–161, 2018.

[7] N. Mohammad Yazid, A. H. M. Din, M. F. Pa'suya, A. H. Omar, N. Mohamad Abdullah, and M. H. Hamden, "The optimization of marine geoid model from altimetry data using Least Squares Stokes modification approach with additive corrections across Malaysia," *Int J Remote Sens*, pp. 1–27, 2023.

[8] M. J. Fernandes, L. Bastos, and J. Catalão, "The role of multi-mission ERS altimetry in the determination of the marine geoid in the Azores," *Marine Geodesy*, vol. 23, no. 1, pp. 1–16, 2000.

[9] F. Sansò and M. G. Sideris, *Geoid determination: theory and methods*. Springer Science & Business Media, 2013.

[10] C. Hwang *et al.*, "New gravimetric-only and hybrid geoid models of Taiwan for height modernisation, cross-island datum connection and airborne LiDAR mapping," *J Geod*, vol. 94, pp. 1–22, 2020.

[11] D. T. Sandwell and W. H. F. Smith, "Marine gravity anomaly from Geosat and ERS 1 satellite altimetry," *J Geophys Res Solid Earth*, vol. 102, no. B5, pp. 10039–10054, 1997.

[12] Z. Li, J. Guo, B. Ji, X. Wan, and S. Zhang, "A review of marine gravity field recovery from satellite altimetry," *Remote Sens (Basel)*, vol. 14, no. 19, p. 4790, 2022.

[13] C. Hwang, "Inverse Vening Meinesz formula and deflection-geoid formula: application to prediction of gravity and geoid determination over South China Sea," *J Geod*, vol. 72, pp. 113–130, 1998.

[14] Z. Gharineiat and X. Deng, "Spectral analysis of satellite altimeter and tide gauge data around the Northern Australian Coast," *Remote Sens (Basel)*, vol. 12, no. 1, p. 161, 2020.

[15] J. Calman, "Introduction to sea-surface topography from satellite altimetry," *Johns Hopkins APL Tech Dig*, vol. 8, no. 2, pp. 206–210, 1987.

[16] F. Sansò, G. Venuti, I. N. Tziavos, G. S. Vergos, V. N. Grigoriadis, and G. Vergos, "Geoid and Sea Surface Topography from satellite and ground data in the Mediterranean region-A review and new proposals," *Bulletin of Geodesy and Geomatics*, vol. 67, no. 3, pp. 155–201, 2008.

[17] B. Hofmann-Wellenhof and H. Moritz, *Physical geodesy*. Springer Science & Business Media, 2005.

[18] L.-L. Fu and A. Cazenave, *Satellite altimetry and earth sciences: a handbook of techniques and applications*. Elsevier, 2000.

[19] W. Bosch and R. Savcenko, "On estimating the dynamic ocean topography–a profile approach," in *Gravity, Geoid and Earth Observation: IAG Commission 2: Gravity Field, Chania, Crete, Greece, 23-27 June 2008*, Springer, 2010, pp. 263–269.

[20] R. E. Haagmans, "Fast evaluation of convolution integrals on the sphere using 1D FFT, and a comparison with existing methods for Stokes' integral," *man. geod.*, vol. 18, pp. 227–241, 1993.

[21] Y. M. Wang, "GSFC00 mean sea surface, gravity anomaly, and vertical gravity gradient from satellite altimeter data," *J Geophys Res Oceans*, vol. 106, no. C12, pp. 31167–31174, 2001.

[22] F. Hernandez and P. Schaeffer, "Altimetric mean sea surfaces and gravity anomaly maps inter-comparisons," *AVISO Tech. Rep. AVI-NT-011-5242-CLS, Cent. Natl. d'Etudes Spatiales, Toulouse, France*, 2000.

[23] H. Xu, Y. Tian, J. Yu, O. B. Anderson, Q. Wang, and Z. Sun, "Comparative Study on Predicting Topography from Gravity Anomaly and Gravity Gradient Anomaly," *Remote Sens (Basel)*, vol. 16, no. 1, p. 166, 2023.

[24] S. Vignudelli *et al.*, "Satellite altimetry measurements of sea level in the coastal zone," *Surv Geophys*, vol. 40, pp. 1319–1349, 2019.

[25] O. B. Andersen, P. Knudsen, P. A. M. Berry, S. Kenyon, and R. Trimmer, "Recent developments in high-resolution global altimetric gravity field modeling," *The leading edge*, vol. 29, no. 5, pp. 540–545, 2010.

[26] O. B. Andersen, P. Knudsen, and P. A. M. Berry, "The DNSC08GRA global marine gravity field from double retracked satellite altimetry," *J Geod*, vol. 84, pp. 191–199, 2010.

[27] M. Nurhayati and D. D. Wijaya, "Ocean Tides Model in Eastern Indonesian Sea Using Data Assimilation from Altimetry, Tide Gauge, and Hydrodynamic Model," *Jurnal Inotera*, vol. 9, no. 1, pp. 239–249, 2024.